ELSEVIER

Carbohydrate Research 298 (1997) 105–115

CARBOHYDRATE RESEARCH

X-Ray and conformational analysis of arabinan

Akella Radha, Rengaswami Chandrasekaran *

Whistler Center for Carbohydrate Research, Smith Hall, Purdue University, West Lafayette, IN 47907-1160, USA

Received 13 August 1996; accepted in revised form 29 October 1996

Abstract

Fibers prepared from the enzymically debranched plant polysaccharide arabinan, containing (1 → 5)-linked α-L-arabinofuranose residues, produce X-ray diffraction patterns containing concentric rings indicative of a high degree of structural organization. The measured unit cell dimensions and fiber density are consistent with a 2-fold helix passing through each unit cell. According to model-building techniques and energy calculations, a total of seven molecular structures (three with C2′-*endo* and four with C3′-*endo* sugars), all of pitch 8.74 Å, and hence seven different crystal-packing arrangements are the most probable. While intrachain hydrogen bonds are only present in three cases, interhelix association is facilitated by hydrogen bonds in all allomorphs. Small energy differences between them suggest that easy conformational transitions may be made from one form to another. This polymorphism and the tendency to form microcrystals in the solid state might confer upon arabinan the observed fat mimetic properties.

Keywords: Arabinan; X-ray structure; Conformation

1. Introduction

Arabinan is a plant polysaccharide that occurs in the primary cell-walls in association with pectins, as in sugar beet, various seeds, fruits, and roots. Its main chain is composed of (1 → 5)-linked α-L-arabinofuranose residues. It is commonly present as a side chain attached to the rhamnose residues which frequently interrupt the linear galacturonan (i.e., pectate) chains. In nature, arabinan also contains high levels of monosaccharide side-chains of α-L-arabinofuranose residues. Because of the branches, arabinan is freely soluble in water to a high concentration (> 20% w/w). Enzymically debranched arabinan, known as araban, has a DP of 50–80 residues. The solubility of araban extracted from sugar beet is considerably decreased, as it dissolves in water only at an elevated temperature of ~ 95 °C to a concentration between 10 and 20% w/w, and it develops a smooth and spreadable gel, similar to maltodextrins, upon storage at ambient temperature [1,2]. An early chemical and NMR analysis of arabinan obtained from the material precipitated from apple-juice concentrate has suggested that the polymer is linear and its X-ray pattern is diagnostic of a high degree of order in the powder sample [3].

Araban's ability to match closely the rheological

* Corresponding author. Tel.: +1-317-4944923; fax: +1-317-4947953; e-mail: chandrar@foodsci.purdue.edu.

0008-6215/97/$17.00
PII S0008-6215(96)00289-3

properties of high-fat products has resulted in a considerable number of opportunities for using this ability in fat replacement [1,2]. In low-fat spreads, ice creams, chilled or frozen desserts, at least 50% substitution has already been demonstrated [4]. In addition to its use as a bulking agent in the food industry, araban has potential practical applications in cosmetics, pharmaceuticals, and toiletries [5].

Some interesting physicochemical properties of araban in solution and gels have recently emerged. For example, the concentration dependence of zero-shear viscosity of araban solution prior to gelation [5] is typical of disordered polysaccharide chains interacting by physical entanglement alone [6]. The gel-structure visualized by electron microscopy shows a network of randomly oriented microfibrils around 200 Å in length with a surrounding matrix of finer strands in which initial ordering and later aggregation of the chains is implicated [5]. In another study, the conformational behavior of arabinobiose in aqueous solution has been investigated by high resolution NMR and computerized molecular modeling techniques [7]. For all accessible conformations and for both slow and fast internal motion models, theoretical NMR data have been calculated and compared with the observed parameters. According to these results, no single model yields a good fit, but a conformationally averaged model produces a reasonable match. Extrapolating these conformations to a regular polysaccharide structure, Cros et al. [7] have generated six different n-fold helices (where n, the number of arabinose residues per turn, can be 2, 3, 4, or 6) as probable models for araban; three are left-handed and three right-handed; and the axial rise per residue (h) in them ranges from 2.2 to 4.8 Å.

Based on a preliminary conformational analysis aided by the X-ray diffraction pattern from a polycrystalline and randomly oriented fiber, Chandrasekaran et al. [8] have proposed that araban probably forms a 2-fold helix having $h = 4.37$ Å so that its pitch ($= nh$) is 8.74 Å. In this paper, we confirm this proposal and describe the structural details which have been established subsequently by using a combination of X-ray data, model building techniques, and potential energy calculations. This extended analysis reveals that the araban chain is so flexible that it can adopt up to seven 2-fold helical structures, all with the same pitch noted above. They contrast not only in sugar pucker and molecular conformations, but also in their packing arrangements. Such structural variations constitute the molecular basis of the interesting rheological properties observed for araban.

2. Experimental data

Fiber preparation.—A powder sample of purified araban was provided by the British Sugar Technical Center, Norwich, UK. It was dissolved in water (0.5 mg/mL) at 95 °C with constant stirring. A few drops of this solution were placed in the gap between two glass rods in a fiber puller and allowed to dry slowly under controlled relative humidity. When the material reached a semi-solid state, it was stretched slightly to obtain an intact fiber. The density of the fiber was measured by the flotation method using a mixture of bromoform and benzene.

Diffraction pattern and unit cell contents.—Diffraction pattern was recorded on a flat-film camera using Ni-filtered CuKα radiation ($\lambda = 1.5418$ Å) from a microfocus X-ray generator operated at 40 kV and 6 mA. During exposure to X-rays, the specimen chamber was continuously flushed with helium gas, after it bubbled through a saturated solution of sodium chlorate, in order to maintain the fiber at the desired relative humidity (75%) and to avoid air scattering. The film was calibrated by dusting the fiber with calcite powder (of characteristic d-spacing 3.035 Å) for the measurement of unit cell dimensions. The typical film to fiber distance was 4.2 cm.

The diffraction pattern (Fig. 1) contains a series of concentric rings which differ from each other in intensity and in thickness. It is reminiscent of the powder diffraction patterns commonly observed for minerals. The inference is that the fiber consists of an irregular assembly of microcrystallites having ran-

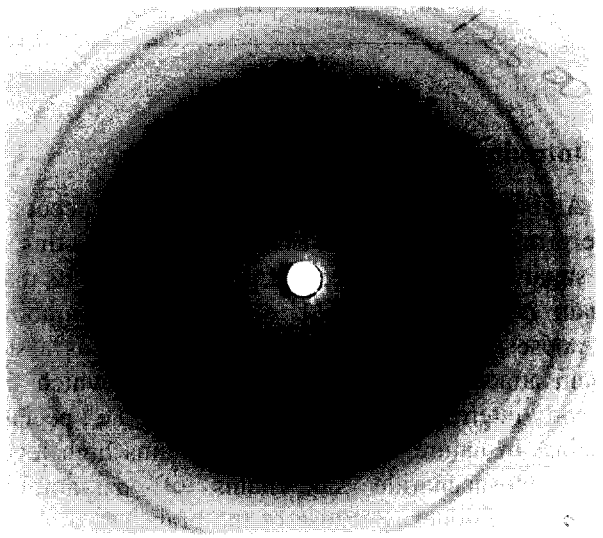

Fig. 1. An X-ray diffraction pattern from araban. The concentric rings indicate considerable structural organization of the polysaccharide chains in the sample.

Table 1
Intensity, Bragg angle, Miller indices, and observed and calculated *d*-spacings of the rings in the diffraction pattern of araban

Ring	Intensity	2θ (°)	*h*	*k*	*l*	d_o (Å)	d_c (Å)
1	W	10.1	0	0	1	8.73	8.74
2	W	14.4	0	1	0	6.13	6.14
3	M	16.0	1	0	0	5.55	5.55
4	VS	17.4	0	1	1	5.09	5.02
5	M	21.0	0	0	2	4.31	4.37
6	M	22.2	1	1	0	3.99	4.12
7	S	23.4	1	1	1	3.81	3.72
8	W	24.7	0	1	2	3.62	3.56
9	VW	29.0	0	2	0	3.09	3.07
10	M	31.0	0	0	3	2.87	2.91
			0	2	1		2.90
11	W	33.6	1	2	0	2.66	2.69
			2	0	1		2.64
			0	1	3		2.63
12	VW	34.5	1	0	3	2.59	2.58
			1	2	1		2.57

VS, S, M, W and VW denote very strong, strong, medium, weak, and very weak, respectively.

dom orientations. This feature is consistent with the low molecular weight of araban (6000–10,000 Da). Such polymers may be trapped as microcrystals, but are otherwise difficult to be preferentially oriented. The twelve rings visible up to 2.6 Å can be indexed (Table 1) with a unit cell of dimensions $a = 5.55$, $b = 6.14$, $c = 8.74$ Å and $\alpha = \beta = \gamma = 90°$. It should be recognized that the qualitative intensities and the *d*-spacings of rings 4, 5, 7, 8, 10 and 12 in this table are in good agreement with those of the first six out of seven rings formerly published by Churms et al. [3]. To fit the measured fiber density of 1.53 g/mL, only two monosaccharide units can be accommodated in this unit cell. If the araban chain adopts a regular structure, it is most likely to be a 2-fold helix whose pitch is *a*, *b*, or *c*, and the space group is probably $P2_1$. The inability to assign the correct pitch stems from the random orientations of the microcrystallites in the diffracting specimen. The solution to this problem is to compute and compare the relative stabilities of sterically feasible helical models in all three cases.

3. Conformational analysis

Generation of acceptable molecular models.—Following the atom labeling of the disaccharide unit shown in Fig. 2, the three major conformation angles that alter the shape of the arabinofuranose residue in a regular helix are ϕ(C-2–C-1–O-5′–C-5′), ψ(C-1–O-5′–C-5′–C-4′) and ω(O-5–C-5–C-4–C-3) where atoms in the reducing end residue are primed. By making use of the matrix method for generating helical structures [9], we determined the *n* and *h* values [10] in the (ϕ, ψ, ω) space; additional input for this procedure related to (*a*) the geometry or coordinates of the monosaccharide unit in an internal frame of reference and (*b*) the bond angle at the glycosidic bridge oxygen atom, which was set at 116.5°.

Evaluation of the potential energy [9] of the helices in isolation allowed us to reject a number of sterically unfavorable structures and concentrate on a few stable conformers only for further analysis. The primary contributions to helix stability arise from nonbonded, electrostatic, and hydrogen-bonding interactions. They were computed with the aid of Lennard Jones 6–12 function, monopole approximation and a modified set of constants [11], respectively. The three preferred domains of ω, surrounding 60, 180, and −60°, were individually explored in order that only ϕ and ψ were treated as the principal variables of the araban helix. This had the merit of computing a two-dimensional (ϕ, ψ) plot, at coarse intervals of 20° initially, containing iso-energy contours, iso-*n* and iso-*h* contours, or superposition of all of them, for a specific value of ω. When required, these maps were also computed at smaller intervals in the low energy domains alone.

Consistent with the flexibility of 5-membered rings, both C2′-*endo* and C3′-*endo* geometries for arabinofuranose, adapted from single-crystal structures [12–

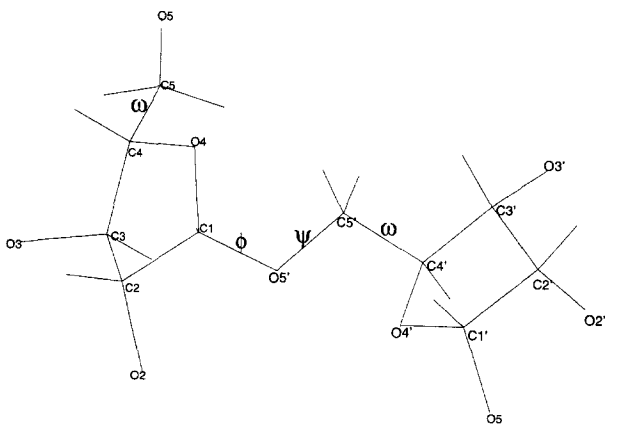

Fig. 2. Schematic drawing of an arabinobiose disaccharide unit showing the three major conformation angles ω, ϕ, and ψ which control the flexibility of the main chain.

14], were independently investigated. Overall, the search for stereochemically-allowed araban helices encompassed the two distinct sugar conformations, each in combination with the three possible staggered domains for ω.

Packing arrangements.—The Linked-Atom Least-Squares (LALS) program [15] was subsequently used to refine the conformation angles of the low energy helices obtained above and their packing arrangements in the unit cell. Since the X-ray intensities from a 'powder' diffraction pattern (Fig. 1) are beyond the scope of this routine, the function minimized in the refinement was of the form

$$\Omega = \sum e_i({}_o\theta_i - \theta_i)^2 + \sum k_j({}_od_j - d_j)^2 + \sum \lambda_h G_h = E + C + L. \quad (1)$$

The first term E restrains each varied conformation or bond angle (θ_i) in the model near a preferred value ${}_o\theta_i$. The second term C optimizes the non-covalent interactions (driving short contacts d_j to larger and acceptable limits ${}_od_j$) and hydrogen bonds within and between helices. The last term L imposes Lagrange constraints G_h and becomes zero when helix connectivity and sugar ring closure are achieved. Note that e_i and k_j are the weights associated with the observations in the first and second terms, respectively. Successful refinement of the previously defined molecular models led to further visualization of the most probable packing modes. The relative stabilities were finally ascertained from their potential energies calculated using the Amber forcefield for non-bonded, electrostatic and hydrogen bonding interactions with the crystal-cell module of the polymer software package (version 7.0) from Biosym Technologies release 2.3.7.

4. Results

Symmetry of the araban helix.—A total of six ab initio energy plots, superposed on iso-*n* and iso-*h* contours, taking into account the two sugar puckers and the three preferred domains for ω, were generally in favor of 2-fold helices in the low energy regions. Interestingly, the most promising models were compatible only with $h = c/2$ (4.37 Å). The remaining two alternates, $h = a/2$ (2.78 Å) and $b/2$ (3.07 Å), are too short to form 2-fold helices in which the length of the O-5 · · · O-5′ virtual bond varies from 4.8 to 5.3 Å due to the rotational freedom about C-4–C-5; therefore, these abortive models were not considered further. Helices with higher symmetry were found to be either less stable in the energy maps or incompatible with the diffraction data. It was hence concluded that a 2-fold helix with $h = 4.37$ Å is the best choice for araban.

Table 2
Major main chain (ω, ϕ, ψ) and sugar ring conformation angles (ν_0 to ν_4), endocyclic bond angles (τ_0 to τ_4), pseudorotation parameters (P and τ_m), and total energy (E) of the araban allomorphs

Parameter	Model						
	1	**2**	**3**	**4**	**5**	**6**	**7**
ω(O-5–C-5–C-4–C-3)	−67	−66	−173	−62	−59	72	−168
ϕ(C-2–C-1–O-5′–C-5′)	74	116	−165	141	54	147	−142
ψ(C-1–O-5′–C-5′–C-4′)	−154	132	−178	120	−119	47	179
ν_0(C-4–O-4–C-1–C-2)	21	8	18	2	4	4	7
ν_1(O-4–C-1–C-2–C-3)	−33	−21	−38	24	20	21	20
ν_2(C-1–C-2–C-3–C-4)	32	26	41	−39	−34	−36	−38
ν_3(C-2–C-3–C-4–O-4)	−21	−21	−33	42	38	40	38
ν_4(C-3–C-4–O-4–C-1)	−1	8	10	−29	−27	−28	−31
τ_0(C-4–O-4–C-1)	111	112	108	108	109	110	114
τ_1(O-4–C-1–C-2)	106	107	108	107	107	107	100
τ_2(C-1–C-2–C-3)	102	104	98	103	103	102	109
τ_3(C-2–C-3–C-4)	104	104	101	98	100	101	97
τ_4(C-3–C-4–O-4)	106	106	106	106	106	104	104
P	161	180	174	22	25	25	26
τ_m	34	27	45	44	40	41	41
Ω	13.8	11.3	20.4	16.3	14.0	17.4	11.2
E (kcal/mole)	−1.1	−3.7	2.3	−2.4	−2.8	−2.4	−2.7

Based on P, the sugar conformational domains are C2′-*endo* in models **1** to **3** and C3′-*endo* in models **4** to **7**.

C2'-endo models.—When the sugar rings have the C2'-*endo* conformations, the $\omega = 60°$ domain is completely prohibited, but the other two domains are satisfactory. There are two distinct models, **1** and **2**, in the $-60°$ domain which are stabilized by intra-chain hydrogen bonds. In contrast, model **3** in the 180° domain does not display hydrogen bonds within the helix. Because of differences in the main chain conformation angles, the three helices remotely resemble each other.

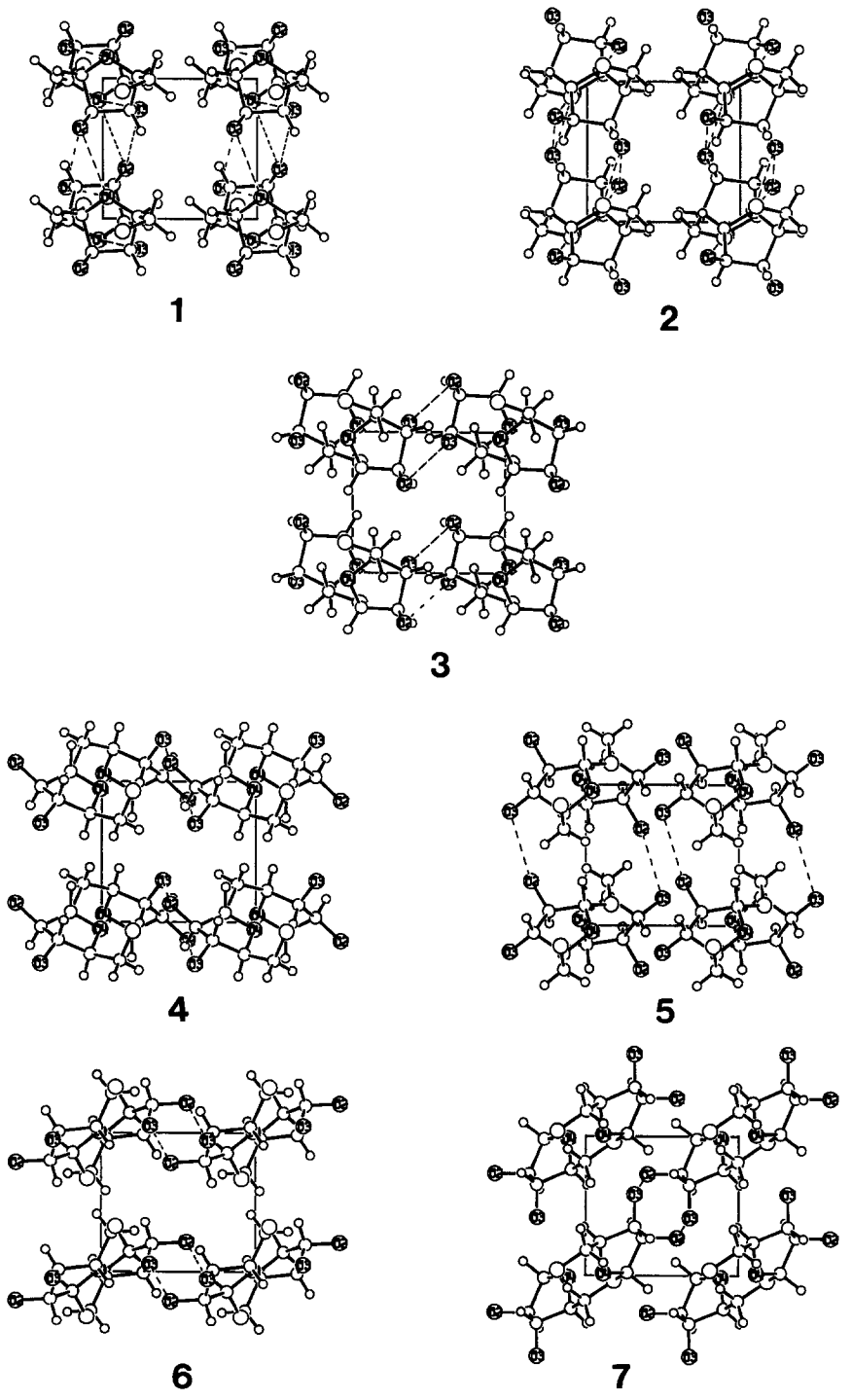

Fig. 3. Packing arrangement of araban helices in the unit cell as viewed along the *c*-axis for models **1** to **7**. The *a*-axis is down and *b*-axis across the page in all cases. The dashed lines are hydrogen bonds which lead to hydrogen bonded sheets along *a*, *b*, or the diagonal.

C3′ - endo models.—All the three staggered domains for ω are equally probable when the helix accommodates C3′-*endo* sugar conformations. The $-60°$ domain produces models **4** and **5**, and the 60° and 180° domains generate models **6** and **7**, respectively. Only model **6** sustains any intrachain hydrogen bonds.

Packing arrangements.—The application of the LALS method [15] was crucial for the optimization of helix packing in the unit cell, for the simultaneous refinement of the main chain conformation angles, and for relaxing the sugar geometries for all seven models noted above. The final conformation angles and sugar ring parameters, including those of pseudorotation (phase P and amplitude τ_m), are listed in Table 2. In this, the penultimate row contains the final term [in Eq. (1)], and the last row represents the total energy E per monosaccharide repeat, taking into account intra- and inter-helix interactions in the packing arrangements shown in Fig. 3. Models **2** and **3**

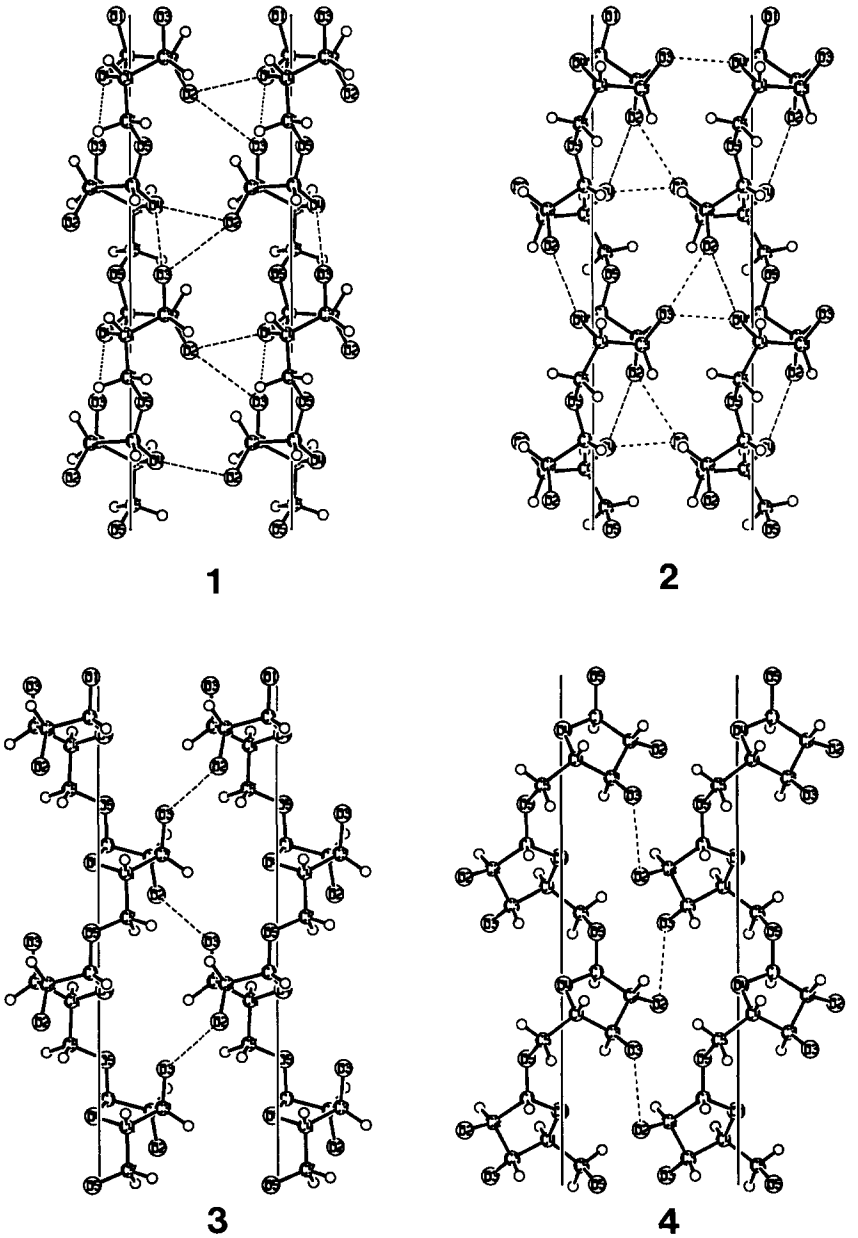

Fig. 4. Longitudinal view of two turns of a pair of helices showing not only the molecular structure but also the association between them in **1** to **7**. Their lateral separation is given in Table 3. The dashed lines are hydrogen bonds and the vertical thin line is the helix axis. For clarity, the ring and glycosidic atoms are labeled, and hydrogen atoms are unmarked. Note that intrahelical hydrogen bonds exist only in **1**, **2**, and **6**.

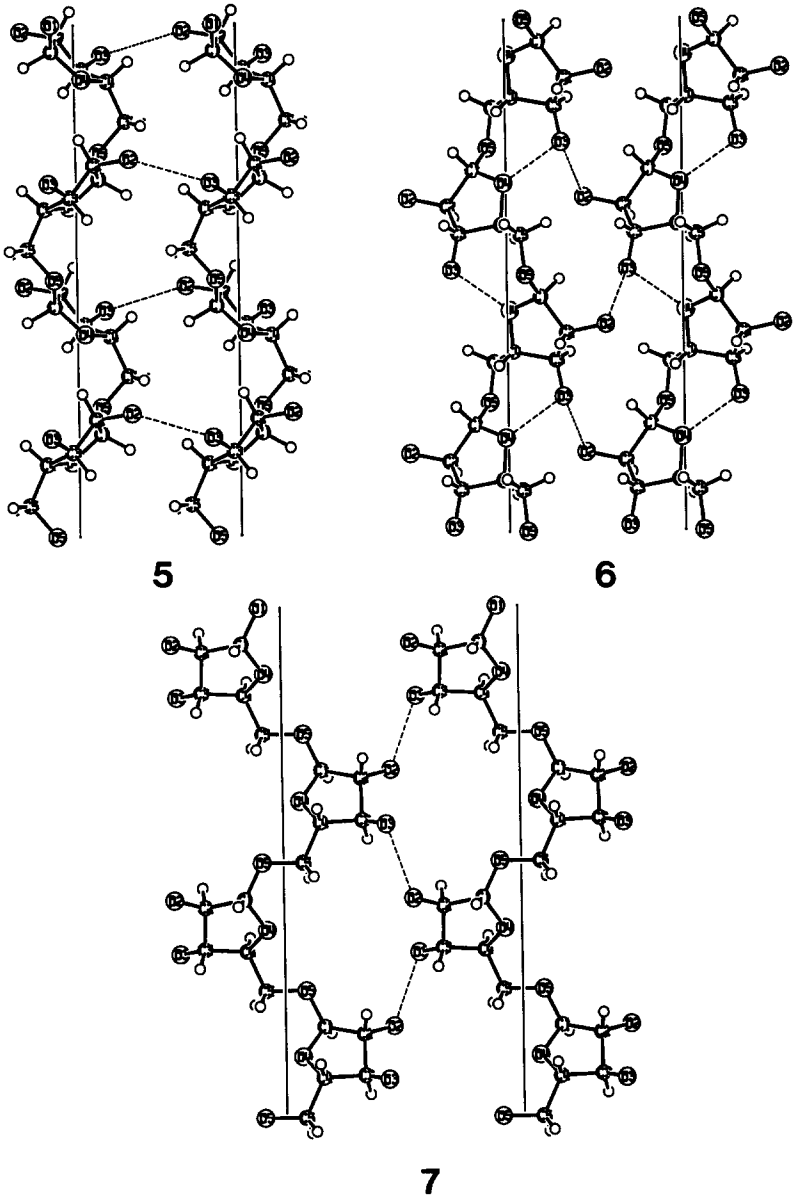

Fig. 4 (continued).

have the lowest and highest energies, −3.7 and 2.3 kcal/mol, respectively; others have intermediate energies. In general, both Ω and E follow the same trend in predicting relative stabilities of the models.

Molecular features.—Side views of the family of seven helices for araban, all having $n = 2$ and $h =$ 4.37 Å, are illustrated in Fig. 4. Each panel depicts the association of adjacent helices in the crystalline arrangement by interchain hydrogen bonds. Inspection of these drawings brings out several interesting observations. First, no two helices look alike since the conformation angles assume characteristic values for each model. Second, all the helices are right-handed, except for **1** and **6** which are both left-handed. This may be perceived in Fig. 4 by following the trajectory of the sequence O-5–C-5–C-4–O-4–C-1–O-5′ along a chain. Third, the positioning of the helix axis relative to the polysaccharide chain is not the same in every case. For example, the sugar rings are astride the helix axis in **1** and **2**, but they are away from this axis to varying extents in the rest. This effect is most pronounced in **7**. The peripheral hetero atom in any of these models is within 4.0 Å from the helix axis.

Fourth, the C2′-*endo* sugar rings in **1** to **3** are located approximately in the horizontal plane so that

the segment C-1–O-5–C-5–C-4 spans the axial rise h; this is accomplished easily since ψ is in the *trans* domain. On the other hand, the C3′-*endo* sugar rings in **4** to **7** have quite different orientations. The trend is that they are inclined towards the helix axis. This effect is best perceived in **6** where the C-4–O-4 bond is aligned vertically.

The fifth and final observation is that **1**, **2**, and **6** exhibit intrachain hydrogen bonds 3OH · · · O-4′, 2OH · · · O-4 and 3OH · · · O-4, respectively (Table 3). In isolation, therefore, the remaining helices which lack similar attractive interactions connecting adjacent residues might be less favored.

Intermolecular interactions.—The two free hydroxyl groups 2-OH and 3-OH in the arabinofuranosyl unit are exploited extensively in the short range lateral organization of araban helices. This is clearly demonstrated in Fig. 3. The panels illustrate no similarities among the seven models. However, three distinct modes of association between the helices are obvious. In the first, helices are connected by hydrogen bonds along the a-direction of the unit cell in **1**, **2**, and **5**. In the second, similar association takes effect along the b-axis as observed in **3**, **4**, and **6**. The third mode is unique to **7** only in which the helices joined by hydrogen bonds are 8.3 Å apart, along the diagonal of ab-plane of the unit cell. The panels in Fig. 4 reiterate the same observations from another view which is normal to the polysaccharide chains. The details of the hydrogen bonds are given in Table 3. The atomic coordinates are listed in Table 4.

Table 3
Intra- and inter-helical hydrogen bonds in the low energy allomorphs of araban

Model	Interaction	Donor X	Acceptor Y	Precursor P	X · · · Y (Å)	P–X · · · Y (°)
1	Intra	3OH	O-4′	C-3	2.91	130
	Inter	2OH	O-4(10)	C-2	2.98	97
		3OH	O-2(10)	C-3	3.00	120
2	Intra	2OH	O-4	C-2	2.82	132
	Inter	3OH	O-4(10)	C-3	2.70	114
		3OH	O-2(10)	C-3	2.82	158
3	Inter	3OH	O-2(01)	C-3	2.93	137
4	Inter	3OH	O-2(01)	C-3	2.96	105
5	Inter	3OH	O-2(10)	C-3	3.00	114
6	Intra	3OH	O-4	C-3	2.50	112
	Inter	2OH	O-3(01)	C-2	2.55	116
7	Inter	3OH	O-2(11)	C-3	2.70	113

The two digits in parenthesis following atom Y define the translation of the acceptor helix from the donor along the unit cell edges a and b, respectively.

5. Discussion

The three-dimensional structure of araban has remained elusive for quite sometime for various reasons. If its low molecular weight is a major impediment to detailed X-ray fiber diffraction analysis, the lack of other experimental observations has certainly made it more difficult to determine the molecular structure by conformational analysis alone. For example, the elegant study based on molecular dynamics coupled with NMR spectra on arabinobiose reported six possible (2, 3, 4, and 6-fold) helical models for the polymer in which h varied from 2.2 to 4.8 Å [7]. While two of them with C3′-*endo* sugars and one with a C2′-*endo* sugar were left-handed, the other three with C2′-*endo* sugars formed right-handed structures. Identification of the correct helix type was beyond this work [7].

Our X-ray experiments did not generate a 'fiber' diffraction pattern containing Bragg reflections that would be ideal for solving the 'crystal' structure in order that the structure–function relationship could be understood. Instead, every stretched araban fiber produced only a 'powder' pattern which is the least suited for biopolymer investigation, but the d-spacings of the diffraction rings were extremely crucial (a) to assign the most probable unit cell for the microcrystallites, (b) to define the symmetry of the chain to be a 2-fold helix so that higher symmetry helices are only frail options, and (c) to confine the helix pitch to the unit cell edge a, b or c.

The utilization of this new and powerful information in subsequent conformational analysis has confirmed that the pitch of any 2-fold helix should be 8.74 Å ($= c$). Coupled with C2′-*endo* or C3′-*endo* sugar pucker throughout the chain, seven different molecular structures, and hence seven packing arrangements, are energetically preferred in the crystalline state and they cannot be discriminated easily. Because of the three single bond rotations (ω, ϕ, ψ) per monosaccharide residue, the flexibility of the araban chain will persist in the solid, solution and gel states. Consequently, adjacent residues may not be conformationally identical in some molecules. Such a relaxation would no longer support the monoclinic space group $P2_1$. Instead, triclinic P1 is more appropriate. This is evident from the occurrence of 001 (weak) and 003 (part of an overlapping medium) reflections (Table 1) in the diffraction pattern.

The fact that the energies of the seven models are close to each other supports the hypothesis that conversion among conformers is simple. For example,

Table 4
Cartesian and cylindrical polar coordinates of a repeating unit of araban

Model	Atom	x (Å)	y (Å)	z (Å)	r (Å)	ϕ (°)
1	C-1	0.1386	−0.8371	3.0312	0.8485	−80.60
	C-2	−1.3457	−0.4389	2.9492	1.4155	−161.94
	C-3	−1.2548	1.0859	2.9876	1.6594	139.13
	C-4	0.0764	1.3944	2.2883	1.3965	86.86
	C-5	−0.0286	1.8325	0.8450	1.8327	90.89
	O-2	−1.9756	−0.9002	1.7679	2.1710	−155.50
	O-3	−1.2234	1.4595	4.3583	1.9044	129.97
	O-4	0.8561	0.1704	2.3607	0.8729	11.26
	O-5	−0.5077	0.7762	0.0000	0.9275	123.19
	H-1	0.2878	−1.8027	2.5259	1.8255	−80.93
	H-2	−1.8668	−0.7981	3.8490	2.0302	−156.85
	H-3	−2.0834	1.5133	2.4039	2.5750	144.01
	H-4	0.5958	2.1701	2.8702	2.2504	74.65
	H-51	0.9575	2.1672	0.4905	2.3693	66.16
	H-52	−0.7057	2.6963	0.7720	2.7871	104.67
2	C-1	−0.2504	−0.6468	3.0329	0.6936	−111.16
	C-2	−1.5375	−0.5678	2.1930	1.6390	−159.73
	C-3	−1.7403	0.9266	1.9470	1.9716	151.97
	C-4	−0.3307	1.5233	2.0617	1.5588	102.25
	C-5	0.3592	1.8290	0.7515	1.8639	78.89
	O-2	−1.4095	−1.2892	0.9812	1.9102	−137.55
	O-3	−2.5920	1.3961	2.9830	2.9441	151.69
	O-4	0.4545	0.5482	2.7991	0.7121	50.34
	O-5	0.6303	0.6369	0.0000	0.8961	45.30
	H-1	0.3518	−1.5057	2.7015	1.5462	−76.85
	H-2	−2.3655	−0.9544	2.8054	2.5508	−158.03
	H-3	−2.1194	1.0749	0.9251	2.3764	153.11
	H-4	−0.3968	2.4411	2.6644	2.4731	99.23
	H-51	1.3017	2.3612	0.9477	2.6962	61.13
	H-52	−0.2710	2.5040	0.1538	2.5186	96.18
3	C-1	−1.4030	0.3534	2.9960	1.4468	165.86
	C-2	−1.4796	1.8401	2.6058	2.3612	128.80
	C-3	0.0113	2.1653	2.6855	2.1653	89.70
	C-4	0.6239	0.9155	2.0381	1.1079	55.73
	C-5	0.7668	0.9611	0.5335	1.2295	51.42
	O-2	−2.0036	2.0812	1.3126	2.8889	133.91
	O-3	0.3653	2.2693	4.0577	2.2985	80.85
	O-4	−0.2481	−0.1882	2.4020	0.3114	−142.81
	O-5	1.1997	−0.2987	0.0000	1.2363	−13.98
	H-1	−2.2888	−0.1731	2.6108	2.2953	−175.68
	H-2	−2.0215	2.4133	3.3724	3.1481	129.95
	H-3	0.2456	3.0481	2.0726	3.0580	85.39
	H-4	1.6193	0.8327	2.4988	1.8209	27.21
	H-51	1.4884	1.7440	0.2570	2.2928	49.52
	H-52	−0.1969	1.2392	0.0818	1.2547	99.03
4	C-1	0.3792	−1.2268	2.9801	1.2841	−72.82
	C-2	−0.2084	−2.4031	2.1650	2.4121	−94.96
	C-3	−0.7149	−1.7188	0.8985	1.8616	−112.58
	C-4	−1.2671	−0.4547	1.5440	1.3462	−160.26
	C-5	−1.5175	0.7284	0.6481	1.6832	154.36
	O-2	0.7211	−3.4179	1.8869	3.4931	−78.09
	O-3	−1.6574	−2.4309	0.3048	2.9421	−124.29
	O-4	−0.2901	−0.0569	2.5331	0.2956	−168.90
	O-5	−0.3654	1.2387	0.0000	1.2915	106.43
	H-1	1.4049	−1.2018	2.6120	1.8488	−40.54
	H-2	−0.9526	−2.8256	2.6822	2.9819	−108.63

Table 4 (continued)

Model	Atom	x (Å)	y (Å)	z (Å)	r (Å)	ϕ (°)
4	H-3	0.0484	−1.4993	0.2910	1.5001	−88.15
	H-4	−2.1281	−0.6909	1.9945	2.2374	−162.01
	H-51	−1.9041	1.4765	1.1874	2.4095	142.21
	H-52	−2.1649	0.4699	−0.0688	2.2153	167.75
5	C-1	0.7723	−0.0422	3.4665	0.7735	−3.13
	C-2	0.5389	−1.4940	3.9471	1.5882	−70.17
	C-3	−0.3232	−2.0988	2.8426	2.1235	−98.75
	C-4	−1.1440	−0.8810	2.4391	1.4439	−142.40
	C-5	−1.7569	−0.8828	1.0646	1.9662	−153.32
	O-2	1.7277	−2.2132	4.1491	2.8077	−52.02
	O-3	−1.0759	−3.0734	3.3234	3.2563	−109.29
	O-4	−0.2420	0.2466	2.5158	0.3455	134.46
	O-5	−0.8307	−1.0126	0.0000	1.3097	−129.37
	H-1	1.7206	−0.1408	2.9382	1.7264	−4.68
	H-2	0.0593	−1.4747	4.8244	1.4759	−87.70
	H-3	0.2620	−2.3947	2.0876	2.4090	−83.76
	H-4	−1.8800	−0.7718	3.1071	2.0323	−157.68
	H-51	−2.2489	−0.0243	0.9199	2.2490	−179.38
	H-52	−2.3774	−1.6649	1.0081	2.9024	−145.00
6	C-1	−0.7953	−1.1307	3.6176	1.3824	−125.12
	C-2	−1.1068	−2.0125	2.3853	2.2968	−118.81
	C-3	0.0514	−1.6855	1.4470	1.6863	−88.25
	C-4	0.2366	−0.2003	1.7286	0.3100	−40.25
	C-5	1.5697	0.4088	1.3869	1.6221	14.60
	O-2	−1.1892	−3.3846	2.6719	3.5874	−109.36
	O-3	−0.2951	−1.9182	0.1926	1.9408	−98.75
	O-4	0.0591	−0.0931	3.1596	0.1103	−57.59
	O-5	1.8164	0.5619	0.0000	1.9013	17.19
	H-1	−0.2108	−1.8168	4.2304	1.8290	−96.62
	H-2	−1.9879	−1.7446	1.9956	2.6449	−138.73
	H-3	0.8603	−2.2010	1.7297	2.3632	−68.65
	H-4	−0.4733	0.3201	1.2541	0.5714	145.93
	H-51	2.3009	−0.1680	1.7511	2.3070	−4.18
	H-52	1.6329	1.3189	1.7965	2.0990	38.93
7	C-1	0.1169	1.6719	3.1277	1.6760	86.00
	C-2	1.5124	2.2851	2.8634	2.7403	56.50
	C-3	1.9326	1.9772	1.4291	2.7648	45.65
	C-4	1.3269	0.5814	1.3604	1.4487	23.66
	C-5	1.0058	0.0316	−0.0032	1.0063	1.80
	O-2	1.4969	3.6636	3.1298	3.9576	67.77
	O-3	3.2467	1.9607	1.2862	3.7928	31.13
	O-4	0.0831	0.7061	2.0872	0.7110	83.29
	O-5	0.2106	−1.1413	0.0000	1.1606	−79.54
	H-1	−0.5353	2.5126	2.8914	2.5690	102.03
	H-2	2.1309	1.8682	3.5296	2.8339	41.24
	H-3	1.4780	2.5903	0.7829	2.9823	60.29
	H-4	1.9314	−0.0675	1.8224	1.9326	−2.00
	H-51	1.8563	−0.1941	−0.4783	1.8664	−5.97
	H-52	0.5070	0.7205	−0.5292	0.8810	54.86

Coordinates of the next repeating unit are $(-x, -y, z + 4.37)$ or $(r, \phi + 180, z + 4.37)$.

the transition from **1** to **2** can be induced by breaking the intrachain hydrogen-bond 3-OH · · · O-4′ in favor of making 2-OH · · · O-4 through a change of 42 and 74° in ϕ and ψ, respectively. The interchain hydrogen bond 2-OH · · · O-4 in **1** is replaced by 3-OH · · · O-4. Since both **1** and **2** retain the interchain 3-OH · · · O-2, atom O-3 in each case has bifurcated donor roles in hydrogen bonds. In **3**, **4**, **5**, and **7**, the

absence of intrachain hydrogen bonds lends additional flexibility to the helices, but the formation of hydrogen bonds between helices (Table 3) disciplines lateral organization and enhances structural stability. The keen competition between flexibility of the main chain and interhelical association through hydrogen bonds involving the free hydroxyl groups in the arabinose residues, as seen from the seven models, is unfortunately detrimental to long range lateral organization. The end effect is the formation of microcrystallites exhibiting random orientations.

Although the Rietveld refinement of using powder diffraction data has been very successful in solving the crystal structures of several complex minerals [16], certain limitations of this procedure are nonconductive for the treatment of helical polymers. Likewise, powder samples are beyond the scope of the LALS program which is designed only for 'oriented' systems containing the molecular axes aligned nearly parallel to each other. Under these circumstances, further adjudication among the above seven crystalline allomorphs of araban is meaningless, or difficult, to say the least. Despite this shortcoming, the results gathered so far are in accord with the persistence of randomly oriented microcrystallites (in several araban fibers) which may adopt up to, or perhaps more than, seven distinct packing arrangements. This behavior is crystal clear testimony to polymorphism, similar to that commonly observed in triacylglycerides [17] which are the major constituents of fat molecules. Hence, we believe that this polymorphism in short polysaccharide chains, coupled with easy transitions among the allomorphs, is largely responsible for the previously reported fat mimetic properties of araban [5].

Acknowledgements

This research was partly supported by the Industrial Consortium of the Whistler Center for Carbohydrate Research.

References

[1] J.F. Thibault, F. Guillon, and F.M. Rombouts, in G.O. Phillips, P.A. Williams, and D.J. Wedlock (Eds.), *The Chemistry and Technology of Pectin Industry 6*, Academic Press, London, 1991, pp 119–133.
[2] S. Kasapis, E.R. Morris, and I.T. Norton, in G.O. Phillips, P.A. Williams, and D.J. Wedlock (Eds.), *Gums and Stabilizers for the Food Industry 6*, IRL Press, Oxford, 1992, pp 419–428.
[3] S.C. Churms, E.H. Merrifield, A.M. Stephen, D.R. Walwyn, A. Polson, K.J. van der Merwe, H.S.C. Spies, and N. Costa, *Carbohydr. Res.*, 113 (1983) 339–344.
[4] B.V. McCleary, J.M. Cooper, and E.L. Williams, *British Patent No. 8828378*, 1989.
[5] J.M. Cooper, B.V. McCleary, E.R. Morris, R.K. Richardson, W.M. Marrs, and R.J. Hart, in G.O. Phillips, P.A. Williams, and D.J. Wedlock (Eds.), *Gums and Stabilisers for the Food Industry 6*, IRL Press, Oxford, 1992, pp 451–460.
[6] E.R. Morris, in G.O. Phillips, P.A. Williams, and D.J. Wedlock (Eds.), *Gums and Stabilisers for the Food Industry 2*, IRL Press, Oxford, 1984, pp 57–78.
[7] S. Cros, A. Imberty, N. Bouchemal, C.H.D. Penkoat, and S. Pérez, *Biopolymers*, 34 (1994) 1433–1437.
[8] R. Chandrasekaran, A. Radha, E.J. Lee, and M. Zhang, *Carbohydr. Polymers*, 25 (1994) 235–243.
[9] G.N. Ramachandran and V. Sasisekharan, *Adv. Protein Chem.*, 23 (1968) 347–367.
[10] M. Zhang, M.S. Thesis, Purdue University (1993).
[11] G. Nemethy, M.S. Pottle, and H.A. Scheraga, *J. Phys. Chem.*, 87 (1983) 1983–1987.
[12] P.P. Tougard and O. Lefebrve-Soubeyran, *Acta Crystallogr.*, B30 (1974) 86–89.
[13] J.S. Sherfinski and R.E. Marsh, *Acta Crystallogr.*, B30 (1974) 873–878.
[14] V. Swaminathan, M. Sundaralingam, J.B. Chattopadhyaya, and C.B. Reese, *Acta Crystallogr.*, B36 (1980) 828–832.
[15] P.J.C. Smith and S. Arnott, *Acta Crystallogr.*, A34 (1978) 3–11.
[16] J.E. Post and D.L. Bish, *Minerology*, 20 (1989) 277–308.
[17] J.W. Hagemann, in N. Garti and K. Sato (Eds.), *Crystallization and Polymorphism of Fats and Fatty Acids*, Marcel Dekker Inc., New York, 1988, pp 9–95.